Late stage kinetics of a phase separation induced by a cw laser wave in binary liquid mixtures

J. P. Delville,* C. Lalaude, S. Buil, and A. Ducasse†
Centre de Physique Moléculaire Optique et Hertzienne, UMR CNRS–Université No. 5798, Université Bordeaux I, 351 Cours de la Libération, F-33405 Talence Cedex, France
(Received 30 November 1998)

cw laser waves can be used to locally induce phase transitions. We investigate experimentally and theoretically a laser-driven liquid-liquid phase separation in a micellar phase of microemulsion and analyze its late stage kinetics. The medium is optically quenched in composition in the metastable region of the phase diagram. Two processes can lead to these concentration variations: electrostriction and thermodiffusion. The first originates from induced dipolar couplings in a field gradient. The second corresponds to a variation in concentration driven by a small thermal gradient. Since the nucleated droplets are optically trapped by the beam, we show that it becomes possible to experimentally analyze an academic situation, i.e., the diffusion-driven growth of a single droplet in compensated gravity. The late stage of this kinetics can be divided into two parts, a bulk behavior and a regime controlled by the finite transverse size of the beam. The bulk regime is totally analogous to that observed in classical situations ($R \propto t^{1/3}$, where R is the droplet radius and t the time), and the scaling of the amplitudes in terms of reduced length and time scales is in total agreement with the expected behaviors for fluids belonging to the same Ising universality class. Moreover, the Gaussian beam behaves as an optical bottle with ''soft walls'' in which the absence of rigid boundaries, and thus of wetting couplings, allows an intrinsic description of the influence of finite-size effects on the kinetics. The beam size breaks the dynamic universality when the growing domains start to feel it. We experimentally investigate the resulting slowing down, and a diffusion-driven model of the growth inside a laser wave is built for comparison. The good agreement observed for the bulk regime and during its modification induced by finite-size effects opens a promising field for the development of this new application of laser waves to control out-of-equilibrium liquid mixtures. [S1063-651X(99)10005-9]

PACS number(s): 64.70.Ja, 42.50.Vk, 64.75.+g, 64.60.My

I. INTRODUCTION

In recent years, there have been striking advances towards a better understanding of the intrinsic kinetics of phase separation in liquids [1]. Even if considerable success has been achieved in the matching of theoretical behaviors [2] with most of the experimental data, many aspects are still under investigation, particularly those dealing with additional forcing. This forcing is generally used as an externally driven parameter. As a consequence, the number of degrees of freedom of the system increases, giving birth to new thermodynamic states not available otherwise. This aspect can be very important to develop new applications but, surprisingly, can also improve existing knowledge of the basic behaviors of phase separation in classical situations. This has been particularly the case in flow-induced transitions in liquid systems. Flows can induce phase separation [3], phase ordering [4], crystallization [5], and string formation [6], but steady-state shear also appeared to be an extremely efficient tool to investigate nucleation in a quenched binary mixture [7]. However, understanding of these various phenomena is still in an early stage because their theoretical description cannot be deduced from simple free-energy minimization arguments but by macroscopic equations of motion of the appropriate internal degrees of freedom [8].

Unlike the flow case, electric fields offer an alternative way of analyzing external forcing effects using a simple thermodynamical approach. Indeed, since the invention of bubble chambers [9], electric fields have been recognized as a promising tool to modify the thermodynamic properties of fluids and to drive phase transitions in liquid systems. However, owing to the complex interaction between the electric field produced by a moving particle and a supersaturated fluid, the first goal has been to understand field effects at thermodynamic equilibrium. Several experiments have been designed to this end. For example, in 1965 Debye and Kleboth [10] observed a strong decrease in turbidity in near-critical binary fluids subjected to an electric field. This manifestation was attributed to a shift of the critical point induced by the field. This work on electric field effects in critical opalescence was supplemented by a second work devoted to the relaxation time of concentration fluctuations [11]. Due to the importance of electric fields in a considerable number of applications, these seminal papers have triggered increasing and continuing interest in electric field couplings in bulk liquids [12] and fluid interfaces [13]. However, many aspects remain to be explored. Even if electric field influences on the limit of thermodynamical stability [14] and the nucleation processes [15] have also been analyzed to improve the physics involved in bubble chambers, the interaction mechanisms are still insufficiently known and attempts at modeling [16] have been disappointing. Moreover, despite applications in nucleate boiling [17] and thunderstorm formation [18], bubble and droplet growth rate in electric fields evidently needs further characterization. Finally, the theoretical description of the kinetics of phase separation driven by an

*Electronic address: delville@frbdx11.cribx1.u-bordeaux.fr
†Electronic address: aducasse@frbdx11.cribx1.u-bordeaux.fr

electric field [19], or an electric field gradient [20], remains largely to be made.

The present study analyzes these kinetic aspects when the electric field originates from a cw laser wave and the liquid medium is a near-critical binary liquid mixture. As in the case of steady-state shear flow couplings, we show that the description of the dynamics of a phase separation driven by a laser wave also provides fundamental results concerning the intrinsic behaviors of phase-separating systems. The late stage of the domain growth is illustrated by experiments done in a near-critical micellar phase of microemulsion.

In fact, light-induced phase transitions are well known, but laser waves have been essentially used as pressure (optical cavitation [21]) or heating [22] sources. However, none of these experiments, or even more recent investigations on light-induced nucleation in supersaturated solutions [23], have been able to describe the dynamics of the driven transitions. The main reasons are understandable. In optical cavitation, the system is driven in a strong nonlinear regime. For laser-induced heating, the situation could be more tractable from the theoretical point of view; however, owing to the Gaussian nature of laser waves and their high intensities, the gradient of temperature is difficult to control experimentally in absorbing liquids and can lead to complex secondary effects, such as photophoresis [24], which usually strongly disturb (or even destroy) the expected dynamical behaviors. Nevertheless, recent experiments done inside the tightly focused wave of an optical tweezer have shown that phase separation in liquid mixtures can be generated around the focus either by an overheating [25] or an osmotic compression [26] driven by the field distribution. This offers the opportunity to analyze the kinetics of the induced transition and to explore the possibilities of this new application of laser waves. Phase transitions can also be induced by relatively unfocused beams [27]. However, since little has been done in this new area, the subject needs to be investigated more deeply from both the theoretical and the experimental viewpoints. This is the purpose of the present paper.

We describe here a well controlled way to analyze the kinetics of a first-order phase transition driven by a classical laser wave in a binary liquid mixture. The phase separation is induced by a quench in composition via wave-generated local variations in the concentration of one of the components of the mixture. Essentially, two different processes can lead to these variations in composition: electrostriction [28] and thermodiffusion [29]. The former results from the coupling of the induced dipole moment generated by the field on each particle of solute with the gradient of this field. The latter takes into account the following indirect thermal effect. Even with off-resonance laser beams, the wave is always slightly absorbed in the mixture due to a residual absorption of the components. Owing to the Gaussian nature of the wave, a very weak beam-centered thermal gradient is generated. Despite its weakness, it can induce large concentration gradients, particularly in the vicinity of a liquid-liquid critical point where the Soret constant presents a diverging behavior.

As will be theoretically described and experimentally illustrated, the quenching in composition by a laser wave has many advantages. (i) The transition is confined inside the beam. As a consequence, the interaction between domains is essentially one-dimensional during the late stage of the growth [27]. Moreover, if the medium is also confined along the propagation axis, then it becomes simple to analyze the growth of a single domain generated by the wave. In this case, no interaction between nucleated domains needs to be taken into account. (ii) When the size of the growing domains is small compared to the beam diameter, the field coupling is analogous to the standard spatially uniform quench obtained in classical situations. Thus, familiar droplet growth behaviors are still accessible using an electromagnetic wave, and they can be compared to the large set of existing experimental data. (iii) Since the boundaries of the confined transition are the wave edges, the beam behaves as a box with ''soft walls'' and no wetting effects. This allows the analysis of intrinsic finite-size effects on the droplet growth [30], a situation often encountered in numerical simulations and almost impossible to experimentally explore in classical situations due to wetting couplings on rigid boundaries. (iv) The generated droplets are usually trapped inside the quenched region by the dipolar forces induced by the field gradient. Thus, they always grow in optimized conditions. (v) Owing to the simplicity of the resulting confinement, the kinetics of a phase separation driven by the wave can be theoretically derived, and the model can easily be compared to experimental observations.

The paper is organized as follows. In Sec. II, we present the fundamental processes involved during an optical quench in composition driven by a cw laser wave in a binary liquid mixture, and illustrate the efficiency of such a procedure when a critical microemulsion is considered. We also discuss the optical trapping efficiency of laser waves to create a compensated-gravity geometry. In Sec. III we analyze the late stage kinetics of the resulting phase separation and show how to analyze the growth of a single beam-trapped droplet. To incorporate the kinetics of phase transitions induced by a laser wave in a universal scheme, the data are then interpreted in terms of reduced length and time scales for systems belonging to the same Ising universality class. Section IV is devoted to the droplet growth in the presence of wetting-free finite-size effects. After a first illustration, we derive theoretically the droplet growth rate driven by the field and, in particular, characterize the modification of the growth laws induced by the wave confinement. A comparison of the dynamic behaviors resulting from the different mechanisms discussed in Sec. II, as well as those usually observed in classical uniform quench situations, is presented. We also illustrate experimentally the kinetics of crossover induced by the finite size of the wave for different values of the control parameters, and compare observations with predicted droplet growths. We finally conclude in Sec. V and discuss the opportunities offered by this new application of laser waves to analyze the kinetics of first-order phase transitions in liquid mixtures.

II. LASER-DRIVEN PHASE SEPARATION IN NEAR-CRITICAL LIQUID MIXTURES

A. Fundamental processes

Generally, the thermodynamic state of a binary liquid mixture is described by three variables, for instance the temperature T, the volume fraction Φ of the solute (i.e., the concentration), and the hydrostatic pressure. Since we are

interested here in mixtures close to a liquid-liquid critical point submitted to a low power cw laser radiation, global density fluctuations resulting from a field-induced hydrostatic compression will be negligible compared to the field variations of concentration driven by the osmotic compressibility. Therefore, we suppose in the following that the hydrostatic pressure remains constant, even during the application of a laser wave. Let Φ_0 and T_0 denote the value of Φ and T in the absence of an electromagnetic wave, and Φ_E and T_E their field variations. Φ_E and T_E can easily be evaluated at first order with respect to the beam intensity $I(\vec{r})$ by solving the field-modified heat and mass transfer equations [31]. If we analyze the field interaction during periods much larger than thermal and density characteristic time scales of diffusion, we can neglect the time dependence of these equations, which become at steady state

$$\vec{\nabla}^2\Phi(\vec{r})=\vec{\nabla}^2\Phi_E(\vec{r}), \tag{1a}$$

$$\Lambda_{\rm th}\vec{\nabla}^2T_E(\vec{r})+\alpha_a I(\vec{r})=0, \tag{1b}$$

where $\Phi_E(\vec{r})=\Phi_{\rm th}(\vec{r})+\Phi_{\rm el}(\vec{r})$. $\Phi_{\rm th}(\vec{r})$ and $\Phi_{\rm el}(\vec{r})$ are given by

$$\Phi_{\rm th}(\vec{r})=-\frac{\varrho_0}{\varrho_S}\frac{k_T}{T_0}T_E(\vec{r}), \tag{2a}$$

$$\Phi_{\rm el}(\vec{r})=\frac{\varepsilon_0 K_T\Phi_0^2}{2}\left(\frac{\partial\varepsilon}{\partial\Phi}\right)_T|\vec{E}|^2(\vec{r}). \tag{2b}$$

ϱ_0, ϱ_S, α_a, and $\Lambda_{\rm th}$ are, respectively, the initial density, the density of the solute, the absorption coefficient at the wavelength λ used, and the thermal conductivity. $I(\vec{r})=1/2\varepsilon_0\varepsilon v|\vec{E}|^2(\vec{r})$ is the field intensity where $|\vec{E}|^2(\vec{r})$ represents the slowly varying square amplitude of the optical field (i.e., its mean value over one optical period); v is the light velocity in the mixture and ε and ε_0 are, respectively, the dielectric constant and the dielectric permitivity. $\Phi_{\rm th}(\vec{r})$ describes the thermodiffusive variation of concentration driven by the thermal gradient induced by the wave [Eq. (1b)]. The thermodiffusion is characterized by the Soret constant k_T. $\Phi_{\rm el}(\vec{r})$, which is proportional to the osmotic compressibility K_T, describes the osmotic compression of the solute induced by the wave via electrostrictive forces resulting from field gradients.

Owing to the large time scales involved, the stationary limit of the heat and mass transfer equations can be used to describe the intrinsic late stage kinetics of a liquid-liquid phase transition. Such an assumption means that the field variation of composition has reached its steady state before the phase transition occurs. This decoupling is particularly suitable for weak quenches, i.e., in the conditions assumed in the present study, since Eqs. (1a) and (1b) correspond to an evaluation at first order in field intensity. Moreover, this is totally equivalent to classical situations which suppose a thermal (or a pressure) equilibrium after a temperature (or a pressure) quench inside the coexistence curve before the transition begins [1].

To describe how these laser-induced variations in composition can be used to drive a phase separation in a liquid

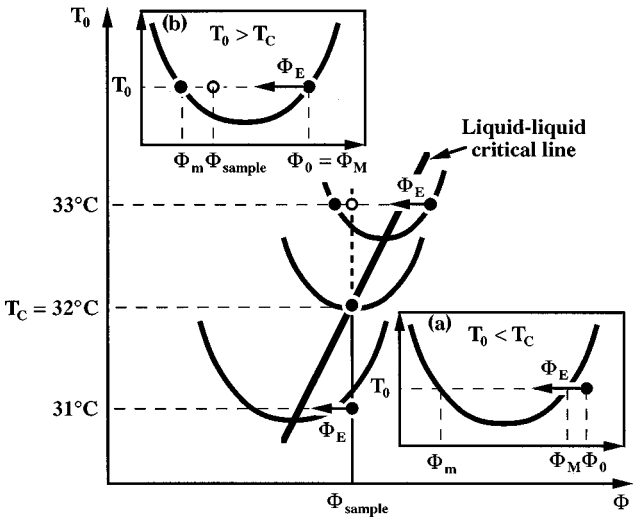

FIG. 1. (a) Schematic phase diagram of our system as a function of temperature T_0 and volume fraction Φ of solute. $\Phi_{\rm sample}$ corresponds to the chosen composition and T_C denotes the critical temperature; Φ_M and Φ_m are, respectively, the concentration of the majority and the minority phases in coexistence. Φ_E represents the local quench in composition induced by the wave from the initial point (Φ_0,T_0). Insets: (a) Situation for $T_0<T_C$ $(\Phi_0=\Phi_{\rm sample})$; (b) situation for $T_0>T_C$ $(\Phi_0=\Phi_M)$.

mixture, let us consider that the electromagnetic field is a classical Gaussian cw laser wave propagating along the z axis. When its beam waist a_0 is relatively large, the beam intensity at the distance r from the propagation axis has almost a cylindrical symmetry, and can be described with the following expression around a_0 ($\rm TEM_{00}$ mode):

$$I(r,z)\approx I(r)=\frac{P}{\pi a_0^2}\exp\left(-\frac{r^2}{a_0^2}\right), \tag{3}$$

where P is the incident beam power. Using Eq. (1b), the laser overheating becomes

$$T_E(r)=\frac{\alpha_a P}{4\pi\Lambda_{\rm th}}\left[-E_1\left(\frac{r^2}{a_0^2}\right)-\ln\left(\frac{r^2}{a_{\rm cl}^2}\right)\right], \tag{4}$$

where $a_{\rm cl}$ is a radius, large compared to a_0, that defines the thermal boundary condition: $T_E(r=a_{\rm cl})=0$. $E_1(x)$ is the 1-argument exponential integral function.

Thus, even if this temperature variation is too weak to be used as a quenching method, as in our low absorption media, the electromagnetic field gradient can locally drive a quench in concentration in a binary liquid mixture located in composition in the vicinity of its coexistence curve [27]. There are two possible scenarios. First, if $\Phi_E(r)<0$, then an increase in the beam power will decrease the solute concentration inside the wave. To induce a phase transition, the initial solute concentration Φ_0 of the mixture will be chosen on the high concentration side of the coexistence curve. This is illustrated by the arrow in Fig. 1, which schematically represents the phase diagram of our system [32] (see below). On the other hand, when $\Phi_E(r)>0$, the quenching procedure is symmetric to the preceding case. Therefore, Φ_0 has to be chosen in the low concentration side of the coexistence curve to drive a phase separation in the system. Due to the thermo-

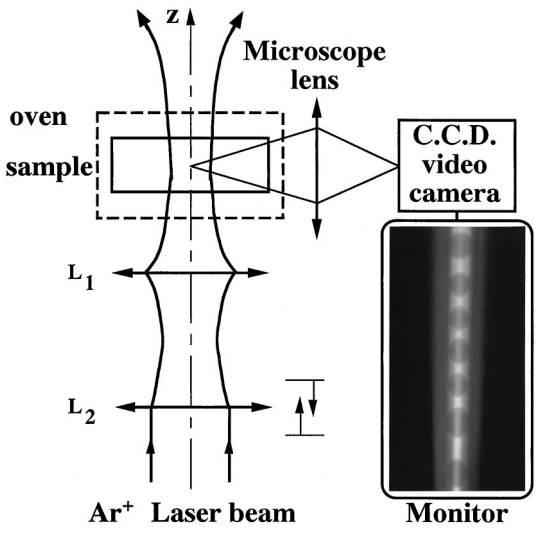

FIG. 2. Experimental setup.

dynamic path followed by these changes in composition, this type of quench is particularly suitable to analyze nucleation and growth processes inside the metastable region of the coexistence curve.

B. Experimental setup and media chosen

The experimental setup used to observe and analyze the induced phase transition is presented in Fig. 2. The liquid mixture is contained in an optical fused quartz cell (1 cm wide, 2 mm thick) placed in a thermally stabilized oven and located at the focus of an X10 microscope lens L_1 which focuses a cw Ar^+ laser beam (wavelength $\lambda_0 = 5145\,\text{Å}$ in vacuum) on the entrance face of the cell ($z=0$). The laser beam propagates vertically through the medium. The evolution of the interaction inside the wave is visualized and recorded transversally to the beam axis, by means of an optical system composed of an X20 microscope lens (numerical aperture of 0.3), a CCD video camera coupled to a VCR, and a personal computer for the frame acquisition. This system also allows us to visualize the beam waist a_0 inside the cell. Values of a_0 ranging from 2 to 20 μm can be achieved by varying the optical path between the two lenses L_1 and L_2 ($f_2 = 200\,\text{mm}$). The brass-made oven is heated by four resistors and the temperature is monitored by a PID; a regulation better than 0.05 K is measured over the cell size.

To experimentally investigate the phase separation induced by concentration variations, we use micellar phases of microemulsions as test media because they are generally sensitive to laser waves. Indeed, owing to the supramolecular size of the micelles, both electrostrictive and thermodiffusive processes can lead to measurable micellar concentration variations on the beam axis [31], and thus are able to induce a phase separation. We consider a quaternary component mixture of water, oil, surfactant (soap), and cosurfactant (alcohol). The selected system has the following mass composition: water 5%, *n*-dodecane 78%, sodium dodecyl sulfate 4.8%, and 1-pentanol 12.2%. The phase diagram has already been reported for the ratio water/surfactant $W/S = 1.034$ used [32]; it is schematically represented in Fig. 1. Located in the oil-rich part of this diagram, our system features a micellar phase at room temperature. This is a stable suspension of surfactant-coated water nanodroplets, called micelles (the solute), in an oil-rich continuum (the solvant). Due to its structure, this quaternary component system is analogous to a binary mixture. From the optical point of view, the micelles can be considered as a set of dielectric spheres suspended in a continuous oil phase. The mixture composition is close to the liquid-liquid coexistence between the critical temperature $T_C = 32\,^\circ\text{C}$ and a demixing temperature $T_D = 20\,^\circ\text{C}$ so that a very small decrease in the micellar concentration induces a liquid-liquid phase separation between two phases of different micellar concentrations (Fig. 1). For $T_0 > T_C$, the system is in a two-phase equilibrium state. As seen below, this does not disturb the experiment because the induced transition is strongly localized in the beam. The latter case, for which Φ_0 becomes the majority phase Φ_M, is particularly interesting because all the incident beam power is used for the quench of the majority phase. For $T_0 < T_C$, a part of the incident beam power is lost for the quench since it brings the system from its initial composition Φ_0 to that corresponding to the crossing of the coexistence curve Φ_M ($\Phi_0 > \Phi_M$).

In this mixture, we have previously shown that the electrostrictive variation in concentration is negligible [27] because the optical polarizability of the micelles is extremely small due to the weak refractive index contrast between water and *n*-dodecane. The interaction between the wave and the micellar phase is mainly controlled by the thermodiffusive process: $\Phi_E(r) = \Phi_{\text{th}}(r)$. Since k_T is positive, thermodiffusion will result in a local decrease in the micellar concentration inside the beam [$\Phi_{\text{th}}(r) < 0$]. In the following, T_0 is considered close to T_C, either $T_0 > T_C$ or $T_0 < T_C$, in order to analyze the kinetic aspects of near-critical phase-separating fluids. Thus, owing to the diverging behavior of the thermodiffusive constant k_T (i.e., $k_T = k_T^0[(T_C - T_0)/T_C]^{-\nu}$ with $k_T^0 \approx 3$ and $\nu = 0.63$) in the vicinity of the critical point, large k_T values can be achieved. As a consequence, despite the very small optical absorption $\alpha_a = 5.58 \times 10^{-4}\,\text{cm}^{-1}$, low cw laser powers are able to induce sizeable concentration variations. In fact, such fluids have many advantages: (i) in the critical region, universality in terms of Ising class is expected [32] and, (ii) the critical divergence of k_T near the critical point allows one to completely neglect the small temperature increase needed for thermodiffusion compared to the associated concentration variation, leading to an almost perfect field-induced quench in composition (limitations linked to the vicinity of the critical point have already been discussed in Ref. [31]).

C. Experimental observation of the induced transition

Without any loss of generality, let us consider the sample for $T_0 < T_C$, i.e., to be a homogeneous micellar phase of microemulsion located in composition close to its coexistence curve [situation depicted in the inset (a) of Fig. 1]. During a beam power increase, the micellar concentration locally decreases. If $|\Phi_{\text{th}}(r)| > \Phi_0 - \Phi_M$, the system is locally driven in the metastable region inside the coexistence curve. For $T_0 > T_C$, i.e., the situation depicted in the inset (b) of Fig. 1, a quench is automatically induced by the application of the laser wave. Typically, at $(T_0 - T_C) = 0.5\,\text{K}$ one finds on the beam axis $T_E(r=0) = 2 \times 10^{-2}\,\text{K}$ and $|\Phi_{\text{th}}(r$

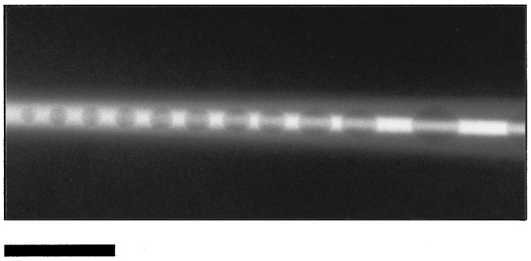

FIG. 3. Droplets generated in the beam by an optical quench in composition in the cell of optical path $l=2$ mm. The control parameters are $P=142$ mW, $a_0=8$ μm, and $T_C-T_0=1.0$ K. The bar length is 100 μm.

$=0)|/\Delta\Phi=5\times10^{-2}$ (where $\Delta\Phi=\Phi_M-\Phi_m$) for $P=150$ mW, $a_{\mathrm{cl}}=100$ μm, and $a_0=8$ μm. This optical quenching in composition of the phase Φ_M results in nucleation inside the beam of droplets constituted by the coexisting minority phase Φ_m, as illustrated in Fig. 3.

Moreover, since the refractive index of the micelles is slightly smaller than that of the surrounding oil, the refractive index of the minority phase Φ_m, and thus of the droplets, is larger than that of the surrounding phase Φ_M. As a consequence, these droplets are transversally trapped in the beam center by the electrostrictive forces and grow in the optically quenched region. The efficiency of this transverse optical trapping compared to the Boltzmann energy k_BT_0 can easily be estimated. Let p_d denote the optical polarizability of a droplet of radius R. In MKSA units one has [33]

$$p_d=4\pi\varepsilon_M\left(\frac{\varepsilon_m-\varepsilon_M}{\varepsilon_m+2\varepsilon_M}\right)R^3, \tag{5}$$

where ε_M and ε_m are, respectively, the dielectric constant of the majority and the minority phases. Therefore, the transverse electrostrictive energy is

$$W_d=-\frac{\varepsilon_0}{2}p_d|\vec{E}|^2. \tag{6}$$

To estimate W_d close to T_C, we assume $\varepsilon_M\approx\varepsilon_m$ and $\Delta\varepsilon=\varepsilon_M-\varepsilon_m=(\partial\varepsilon/\partial\Phi)\Delta\Phi$, where $(\partial\varepsilon/\partial\Phi)=-7.4\times10^{-2}$ was calculated in Ref. [27] using the Clausius-Mossotti relation. At $(T_0-T_C)=0.5$ K, one finds $|W_d|/k_BT_0\approx20$ for a droplet radius $R=1$ μm, $a_0=8$ μm, and a beam power $P=150$ mW. This numerical application shows that the transverse optical trapping is sufficiently strong to allow an efficient droplet growth in the optically quenched region. However, for a slightly focused classical cw laser beam, the axial intensity gradient around a_0 is weak. Thus, the nucleated droplets are nearly free to move along the z direction. This is particularly true when the sample is contained in a thick cell such as that used for the illustration of Fig. 3 (optical path $l=2$ mm). A small ascending flow of the droplets along the beam axis is observed during the late stage of the transition. Although small (measured droplet velocity $V\approx1$ μm/s for a droplet radius $R\approx10$ μm), this advection accelerates the droplet growth which loses its diffusional nature [34]. We will see in the following section how to eliminate this droplet flow in order to describe the growth of a single beam-trapped droplet when it is controlled by diffusion.

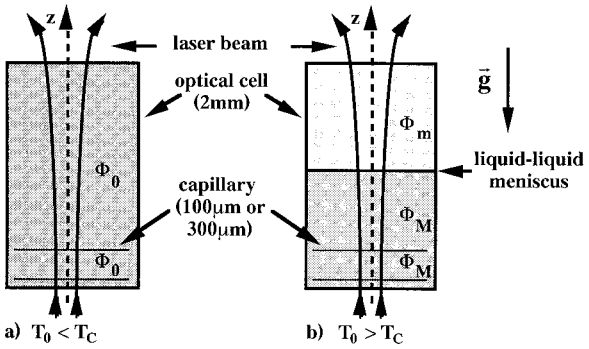

FIG. 4. Experimental configuration. (a) For $T_0<T_C$ (one-phase mixture); (b) for $T_0>T_C$ (phase-separated mixture). $\vec{g}$ represents the gravity field.

III. LATE STAGE DROPLET GROWTH IN LASER-DRIVEN PHASE SEPARATION

A. Growth of a single beam trapped droplet

To preserve a diffusional droplet growth during the late stage of the transition, we axially confined the phase separation using a glass capillary of optical path $l=100$ μm immersed in the fused quartz cell. This experimental configuration is illustrated in Fig. 4, either for $T_0<T_C$ [Fig. 4(a)] or $T_0>T_C$ [Fig. 4(b)]. A typical evolution of the late stage droplet growth in this capillary is illustrated in Figs. 5(a)–5(e). Following an optical quench in composition, we observe the nucleation of several very small droplets (typically five to seven) in the beam. They coalesce by Brownian agitation at the early stage of the transition and give birth to a single droplet [Fig. 5(a)] which grows around the center of the capillary without observable axial movement [Figs. 5(b)–5(e)]. On both sides of this centered droplet, two other hemispherical droplets may be seen to wet the capillary edges (the minority phase of concentration Φ_m is more wettable to glass than the majority phase of concentration Φ_M). These two heterogeneous droplets, which are slightly larger than the beam size, can be evidenced by their curved interfaces, as shown in Fig. 5(a). Their growth, which is also visible in Figs. 5(b)–5(e), induces concentration gradients which generate on the central droplet opposite osmotic forces [34] much larger in modulus than gravity. These forces trap the central droplet axially around the middle of

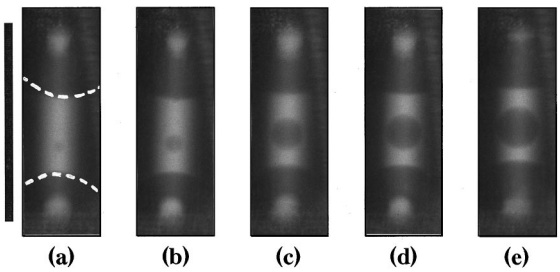

FIG. 5. Droplet generated in the beam by an optical quench in composition in a capillary (100 μm thick) immersed in the cell: (a) $t=100$ s, (b) $t=200$ s, (c) $t=300$ s, (d) $t=500$ s, (e) $t=1000$ s. The two hemispherical droplets wetted on the capillary edges are also underlined in (a). The control parameters are $P=142$ mW, $a_0=8$ μm, and $T_C-T_0=1.0$ K. The bar length is 100 μm.

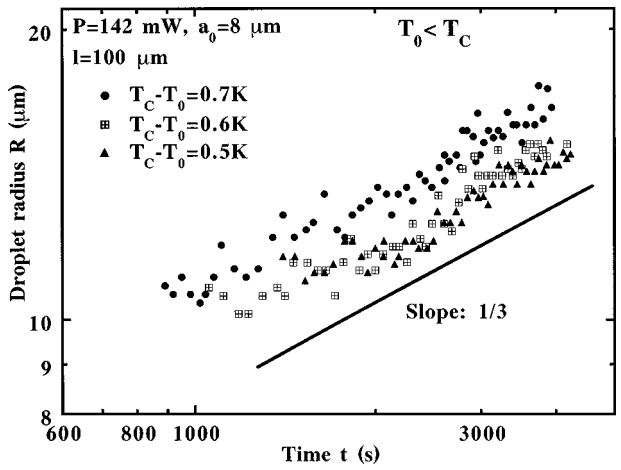

FIG. 6. Bulk behavior of the growth of a single beam-trapped droplet for $T_0<T_C$ in a 100-μm-thick capillary. The bulk regime $R\propto t^{1/3}$ is indicated.

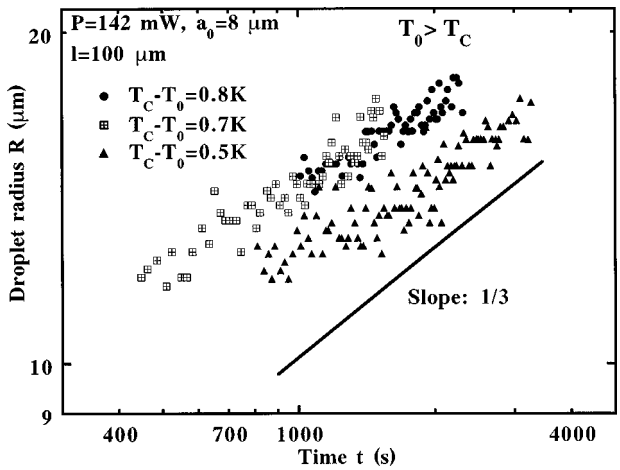

FIG. 7. Bulk behavior of the growth of a single beam-trapped droplet for $T_0>T_C$ in a 100-μm-thick capillary. The bulk regime $R\propto t^{1/3}$ is indicated.

the capillary and totally eliminate the droplet advection during the late stage of the transition. Thus, as long as the droplet does not feel the transverse finite size of the beam, its growth should be analogous to that predicted in classical conserved-order-parameter situations (i.e., bulk behavior in microgravity): $R\propto t^{1/3}$ [35–37], where t is the time. This behavior was investigated for both $T_0<T_C$ and $T_0>T_C$ cases.

Three experiments are presented in Fig. 6 for different positive T_C-T_0 values. All were performed with the same beam radius ($a_0=8\,\mu$m) and incident beam power ($P=142$ mW). The values of these controlled parameters were chosen for several reasons. (i) The beam radius value is sufficiently small to give rise to an efficient transverse trapping of the droplet, and is reasonably large to minimize the divergence of the beam inside the thick cell in order to approximate its shape by a cylindrical Gaussian profile. (ii) The beam power value was chosen to quench the mixture weakly, even if larger beam powers give totally analogous results (see the discussion at the end of this section and Fig. 9). (iii) Finally, both values prevent disturbing secondary effects, such as electrostrictive droplet deformation [38]. The exponents x (defined by $R\propto t^x$) measured for different experiments, including those presented in Fig. 6, are reported in the upper part of Table I. As expected, it can be seen that the droplet radius behaves as $R\propto t^{1/3}$ for $800<t<4000$ s. During this time range, R varies between 9 and 15 μm.

Two points need to be stressed to understand the limitations of these measurements. First, it is very difficult to get reliable results with optical visualization techniques for droplet radii smaller than the beam size. Indeed, even if it is reasonably well trapped, when a droplet is smaller than the beam size, its Brownian motion is still non-negligible. Thus, due to the small field depth of the microscope lens used for the observations, it becomes almost impossible to obtain good images of the droplet is these conditions. Then, it is surprising that droplet radii between 9 and 15 μm do not take fully into account the finite-size effects generated by the Gaussian shape of the wave of beam waist $a_0=8\,\mu$m. In fact, as is theoretically described in the next section, in the presence of thermodiffusion, finite-size effects appear for droplet radii larger than the beam radius. As illustrated by Eq. (4), this is due to the induced temperature distribution at the origin of thermodiffusion, which is much wider than that of the wave. Thermodiffusion is a nonlocal process.

TABLE I. Growth law exponents x ($R\propto t^x$) in the bulk regime and mean value $\overline{x}$ obtained for $T_0<T_C$ (one-phase mixture) and for $T_0>T_C$ (phase-separated mixture).

T_C-T_0 (K)	1.0	0.7	0.6	0.5
x	0.33	0.30	0.32	0.29
$\overline{x}$		0.31		
T_0-T_C (K)	1.0	0.8	0.7	0.5
x	0.25	0.23	0.26	0.23
$\overline{x}$		0.24		

On the other hand, three experiments are presented in Fig. 7 for different positive T_0-T_C values. All were done in the same beam conditions as those performed for $T_0<T_C$ (Fig. 6). The exponents x ($R\propto t^x$) measured for different experiments, including those presented in Fig. 7, are listed in the lower part of Table I. It can be noticed that the observed x are slightly smaller than the expected $x=\frac{1}{3}$ value. This surprising observation may also be explained by the theoretical background developed in the next section. It is a signature of the beginning of the influence of the finite-size effects induced by the Gaussian shape of the wave. Indeed, $\Phi_0=\Phi_M$ for $T_0>T_C$, so all the beam power injected into the medium is used for the optical quenching. As a consequence, for the same $|T_0-T_C|$ and the same beam properties, the quench is deeper than that for $T_0<T_C$. As shown in Sec. IV, the deeper the quench, the faster the droplet saturation towards the thermodynamic equilibrium. Therefore, finite-size effects appear more quickly and slow down the droplet growth faster. This is exactly what is observed here.

B. Data analysis in reduced length and time scales for the Ising class ($d=3$, $n=1$)

The dynamics of phase separation in near-critical systems is a complex problem whose various aspects still remain unsolved. The case of systems belonging to the universality

class ($d=3$, $n=1$) of the Ising model, where d and n are, respectively, the space and the order parameter dimensionalities [1], is the one more commonly studied. It has been the subject of important theoretical and experimental work during the past ten years (see Refs. in [39]). One important goal of these studies is the determination of universal growth laws for the kinetics of the induced phase transitions. To compare the dynamic behavior of very different systems, the experimental data are usually discussed in terms of dimensionless variables reduced from system-dependent length and time scales. However, the comparison between very different systems such as pure fluids, binary liquid mixtures, polymer blends, micellar systems, microemulsions, alloys, and inorganic glasses is made difficult by the puzzling choice of many different characteristic scales. Besides, the conditions in which the phase separation dynamics occurs are not always well known. Moreover, the interaction between growing domains as well as the coupling with an external field, such as gravity, for instance, can strongly bias the analysis of the data. In this section, we present the results of our experiments in which the beam constraint allows the study of the growth of an isolated beam trapped droplet and the optical trapping results in a significant reduction of the gravitational coupling. We compare the dynamic behaviors observed with those of other systems belonging to the same Ising class ($d=3$, $n=1$), using the same scaling.

When a whole system is brought from the one-phase region to the two-phase region, the phase transition may proceed either by droplet nucleation (quench in the metastable region) or by spinodal decomposition (quench in the unstable region). The latter is characterized by a pattern of interconnected domains that interact continuously. Their characteristic size is $L_m(t)=2\pi/k_m(t)$ [40]. This expression is the usual experimental definition of L_m, where k_m is the peak position of the maximum scattered intensity $I(k,t)$ [1]. $L_m(t)$ grows as t^x, where the exponent x evolves as the transition proceeds. The phase separation dynamics of a critical system may be simplified into three main regimes associated with three exponent values: the early stage also known as the Cahn regime ($x\approx 0$), the intermediate stage controlled by diffusion mechanisms ($x\approx\frac{1}{3}$), and the late stage dominated by the hydrodynamic interactions between domains ($x\approx 1$). Classically, two reduced parameters defined as $Q_m(\tau)=k_m(t)/k_m(0)$ and $\tau=t/t_m^0$ are sufficient to compare the behavior of different systems. $[k_m(0)]^{-1}$ is the characteristic length of the chosen system, generally the correlation length of density fluctuations inside the coexistence curve ξ^-, and t_m^0 is the associated relaxation time defined by $(t_m^0)^{-1}=D^-[k_m(0)]^2$, where $D^-=k_BT_0/6\pi\eta\xi^-$ and η are the mass diffusion coefficient and the bulk viscosity.

The first experiments performed on systems of the same molecular nature for different quench depths attempted to show that the evolution of $k_m(t)$ could be plotted on a universal master curve characterized by the boundary condition $(Q_m)^{-1}\rightarrow 1$ when $\tau\rightarrow 0$ [41]. Moreover, Snyder and Meakin [42] compared experimental results obtained for small molecule liquid mixtures, high molecular weight polymers, inorganic glasses, and metallic alloys to determine if there was a common dynamic behavior. All the results seemed to collapse on a single curve $Q_m(\tau)$ for $\tau\rightarrow 0$, with the same asymptotic limit. Their analysis also suggested that, in spite of the large differences between these systems, a similar dynamics governs phase separation processes. To analyze more precisely this suggested scaling behavior, the following analytic function for $Q_m(\tau)$ has been proposed for the early-to-late stage of spinodal decomposition [43]:

$$Q_m^{-1}-1-\left(\frac{A'}{B'}\right)^{1/2}\left\{\tan^{-1}\left[Q_m^{-1}\left(\frac{B'}{A'}\right)^{1/2}\right]-\tan^{-1}\left[\left(\frac{B'}{A'}\right)^{1/2}\right]\right\}=B'\tau. \tag{7}$$

This expression was obtained by integration of the following equation using the boundary condition $(Q_m)^{-1}\rightarrow 1$ when $\tau\rightarrow 0$:

$$\frac{dQ_m^{-1}}{d\tau}=A'Q_m^2+B'. \tag{8}$$

By choosing the correct values for parameters A' and B', Eq. (7) describes the two behaviors $Q_m(\tau)\propto(\tau)^{-1/3}$ and $Q_m(\tau)\propto(\tau)^{-1}$. A' and B' are chosen so as to find the behavior of the early and the intermediate stages predicted by Kawasaki and Ohta [44], and to recover the late stage dynamics calculated by Siggia [45].

Using $Q_m(\tau)=k_m(t)\xi^-$ and $\tau=D^-t/(\xi^-)^2$ [35], the data obtained in the critical case for both pure fluids [46] and binary liquid mixtures [40] show a pattern with interconnected domains associated with a late stage scaled behavior $Q_m(\tau)\propto(\tau)^{-1}$. Moreover, for off-critical systems, a phase separation may proceed by droplet growth, i.e., with a completely different morphology. In that case, recent experiments in binary liquids and pure fluids have pointed to a second late stage scaled behavior $Q_m(\tau)\propto(\tau)^{-1/3}$. An overview of a large number of experiments in relation to these two scaling laws has been presented in Ref. [39]. In spite of an important dispersion in the results, it appears that the experimental behavior $Q_m(\tau)\propto(\tau)^{-1/3}$ described in [35] is the slowest for all these systems, both for interconnected domains and for a compact assembly of droplets.

Our particular case of laser-induced off-critical phase separation belongs to the second type of universal behavior. The growth of the central beam-trapped droplet is described by $R\propto t^x$ with the mean values $\overline{x}=0.31$ and 0.24, respectively, for $T_0<T_C$ and $T_0>T_C$. Moreover, as observed in Fig. 6 and Fig. 7, our results also show that the amplitude of $R(t)$ is, as expected, slightly dependent on the $|T_0-T_C|$ value. This dependence should disappear when data are represented in scaled variables. Figure 8 illustrates the result of this procedure. For the sake of comparison, also represented are the experimental late stage behavior $Q_m(\tau)\propto(\tau)^{-1/3}$ for an off-critical phase separation, analyzed in [35], and the scaled dynamics of spinodal decomposition with its late stage regime $Q_m(\tau)\propto(\tau)^{-1}$. Our data suggest that the reduced growth of a beam-trapped droplet in the bulk regime is comparable to that of a set of tightly packed droplets in microgravity, represented in Fig. 8 by a dashed line. However, even if the slope is in good agreement with the expected behavior for an off-critical liquid, the measured amplitudes are shifted below this limit. More precisely, in this bulk regime $R\propto t^{1/3}$, our experimental data are approximately within

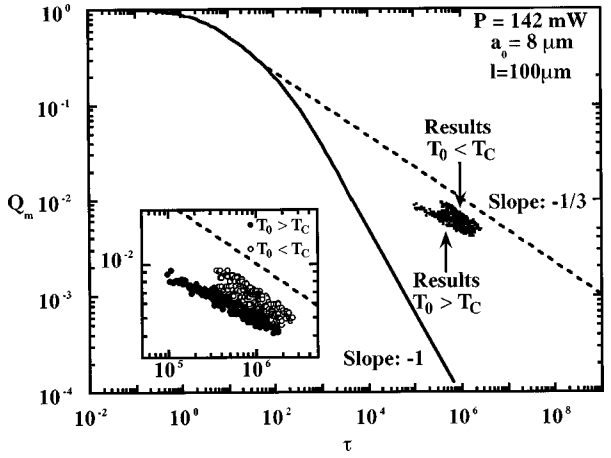

FIG. 8. Representation of the experiments (including those illustrated in Figs. 6 and 7) in reduced variables using the particular choice $Q_m(\tau)=k_m(t)\xi^-$ and $\tau=D^-t/(\xi^-)^2$. For a comparison, the two late stages observed experimentally for systems of the same Ising class, and characterized, respectively, by $Q_m\propto\tau^{-1}$ (critical fluids) and $Q_m\propto\tau^{-1/3}$ (off-critical fluids), are also depicted. Inset: zoom on the measurements to show the relative positions between the data and observations in microgravity.

a factor 2 larger than those obtained in microgravity (mean factor 1.5 for $T_0<T_C$ and 1.8 for $T_0>T_C$). This deviation is not surprising and is due to the droplet coalescences occurring at the early stage of the transition, which momentarily accelerate the kinetics. If we suppose that the observed droplet (characterized by a growth law $R\propto t^{1/3}$) results from the coalescence of N droplets of radius $R_N\propto t^{1/3}$, then roughly $R/R_N=\sqrt[3]{N}$. Factors of 1.5 and 1.8 between R and R_N lead, respectively, to $N=3$ and 6, in agreement with observations ($N\approx 5-7$).

Finally, to show that the choice of $P=142$ mW for the beam power used is not linked to any particularly sensitive property of the medium, except that it corresponds to a weak optical quench condition, Fig. 9 depicts the droplet growth laws observed for much larger beam powers. The $R\propto t^{1/3}$ is still preserved since the measured exponents x ($R\propto t^x$) are $x=0.33$, 0.31, and 0.30, respectively, for $P=230$, 290, and 390 mW. Thus, potentially disturbing secondary effects do not exist for a wide range of beam powers. This underlines the intrinsic robustness of laser-induced transitions and allows a real comparison of the droplet growth behaviors with those obtained in classical uniform situations. Moreover, from this set of experiments one gets the shifts $R/R_N=1.7$, 1.9, and 2.1, respectively, for $P=230$, 290, and 390 mW (see the inset of Fig. 9). As expected, the number of nucleated domains at the beginning of the transition increases with the quench depth (respectively $N=5$, 7, and 9). These experiments show the opportunity provided by optical traps to create a compensated gravity geometry which really preserves a diffusional droplet growth, except during the early coalescence stage.

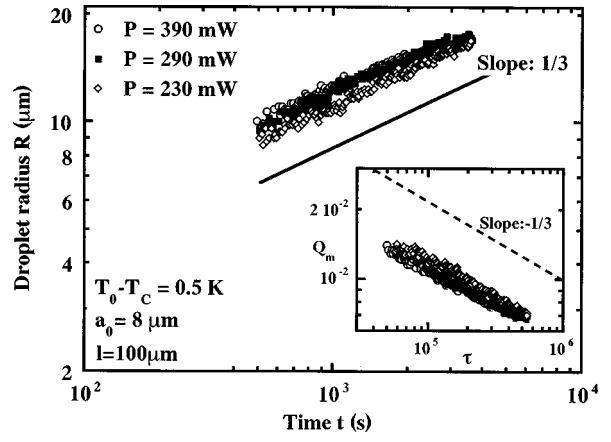

FIG. 9. Illustration of the bulk regime robustness of droplet growth versus the incident beam power. Inset: comparison of the data in reduced variables with the $Q_m\propto\tau^{-1/3}$ behavior observed for off-critical systems (dashed line).

IV. KINETICS OF DROPLET GROWTH IN THE PRESENCE OF WETTING-FREE FINITE-SIZE EFFECTS

A. Experimental evidence of finite-size effects on droplet growth

In the preceding section, we analyzed the existence of the classical bulk regime $R\propto t^{1/3}$ inside a laser wave. This bulk behavior, often considered as the late stage of the transition, does not, in practice, lead to a state of equilibrium. Indeed, a system is always bound and this finiteness will slow the growth down more and more until the system reaches the thermodynamic equilibrium given by the lever rule. Unfortunately, this theoretical expectation, only analyzed numerically [47,48], is difficult to probe experimentally because the late stage of a phase separation is always affected by the preferential attraction of one of the two coexisting phases on the rigid boundaries. This influence of the wetting processes induces hydrodynamic interactions which usually totally modify the droplet pattern, accelerate the kinetics, and destroy the diffusional nature of the growth. By using cw laser waves to quench the mixture, this important problem disappears. Due to the Gaussian shape of the beam, the bulk regime $R\propto t^{1/3}$ cannot indefinitely subsist. As it grows, a droplet probes transversally a region that is less and less quenched by the wave. Thus, after a bulk behavior, the growth will progressively slow down and the droplet radius will reach a maximum value $R^E_{\max}$ defined by the experimental conditions (i.e., beam power, beam radius, and $|T_0-T_C|$). Figure 10 shows this expected crossover between the bulk behavior and that driven by finite-size effects.

B. Theoretical description of the kinetics of a phase separation driven by a cw cylindrical Gaussian wave

After this first experimental illustration, it is of practical importance to build a model for the droplet growth in a Gaussian cw laser wave. For a relatively unfocused laser wave and for axial distances (from the beam-waist location $z=0$) $z_d<2\pi a_0^2/\lambda$, the wave symmetry is almost cylindrical around the propagation axis. In this section we take into account this symmetry of the optical quenching to build a cylindrical model of growth. However, despite this symmetry, Figs. 3 and 4 show that the growing droplets are spherical due to a minimization of the surface energy; rupturing in spheres induced by Rayleigh-like instabilities of growing cy-

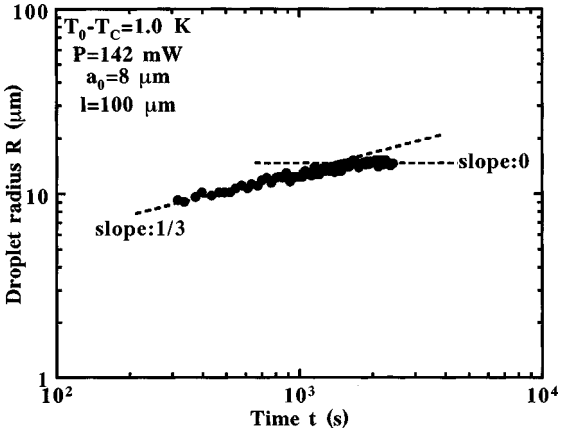

FIG. 10. Experimental late stage growth law of a beam-trapped droplet in the 100-μm-thick capillary. The regimes $R \propto t^{1/3}$ (bulk behavior) and $R \propto t^0$ (saturation of the droplet radius R to $R^E_{\max}$ induced by the finite size of the beam) are indicated.

lindrical droplets in a laser wave has also been observed [49]. Unfortunately, a rigorous treatment of such symmetry mixing (growing spheres in a cylindrical quench), analogous to that encountered for droplet growth in a gravitational field [50], cannot be performed simply. Since our aim is to explore the properties of laser-driven phase transitions and obtain analytical results for easy interpretation of the experimental data, we will not take into account this surface tension effect; instead, we will analyze the transverse growth of cylindrical droplets. To compare the model with the measurements, we will assimilate the predicted radius of the beam centered growing cylinder with that of the observed spherical droplet.

Unlike the spherical symmetry scenario where the single droplet problem may be solved directly from the steady-state equation for the solute diffusion, it is necessary here to consider an effective medium which will remove the unphysical singularity appearing in the concentration field. Indeed, in cylindrical symmetry, the general solution of the stationary mass diffusion equation (1a) exhibits a logarithmic divergence at $r \to \infty$. Even if an *ad hoc* approach towards resolution is to introduce a cutoff distance which prevents this divergence [51], it has been shown [52] that this method leads to incorrect results, even qualitatively. To solve this problem in a more appropriate way, Marqusee [52] considered an effective medium and derived self-consistently the growth rate of circular domains. Thus, we now extend Marqusee's model of two-dimensional Ostwald ripening to the laser-driven transverse growth of a beam-trapped cylindrical droplet of radius R and length l, which is large compared to R ($l \gg R$).

Since the flux of solute $\vec{J}_C(R)$ at the interface of the cylindrical droplet is not known, we postulate its form using that of a spherical quench induced by a spherical wave, and obtain its expression from the boundary conditions. The flux of solute $\vec{J}_S(R)$ around a spherical droplet nucleated in a spherical wave [53] is given by

$$\vec{J}_S(R) = 4\pi R^2 D^- [\vec{\nabla}\Phi]_{\tau=R} = 4\pi R D^- \left\{ \Phi(r\to\infty) - \left(\Phi_R(R) - \left[\frac{\partial}{\partial r}(r\Phi_E(r)) \right]_{r=R} \right) \right\} \frac{\vec{r}}{r}, \tag{9}$$

where $\Phi_E(r)$ is either $\Phi_{\rm el}(r)$ or $\Phi_{\rm th}(r)$ and $\Phi_R(R) = \Phi(r = R)$. Then, we postulate the form of the cylindrical flux as

$$\vec{J}_C(R) = 2\pi R l D^- [\vec{\nabla}\Phi]_{r=R} = l k_E(R) \{ \Phi(r\to\infty) - [\Phi_R(R) - \Psi_E(R)] \} \frac{\vec{r}}{r}, \tag{10}$$

where $k_E(R)$ and $\Psi_E(R)$ are unknown functions which need to be determined. For $r \gg R$, the variation of the solute concentration induced by the droplet growth is given by

$$\frac{\partial}{\partial t}[\Phi_0 - \Phi_E(r\to\infty)] = D^- \vec{\nabla}^2 [\Phi_0 - \Phi_E(r\to\infty)] - \int_0^\infty \left(\vec{J}_C \cdot \frac{\vec{r}}{r} \right) N(R,t)\, dR, \tag{11}$$

where $N(R,t)$ is the density of cylinders of radius R. This solute diffusion equation includes the concentration variation resulting from the growth of other cylinders which constitute an effective medium. Therefore, the intrinsic local concentration of solute $\Phi(r) - \Phi_E(r)$ induced by the growth obeys

$$\frac{\partial}{\partial t}[\Phi(r) - \Phi_E(r)] = D^- \vec{\nabla}^2 [\Phi(r) - \Phi_E(r)] + S_E - D^- (\zeta_E)^{-2} [\Phi(r) - \Phi_E(r)], \tag{12}$$

where

$$D^- (\zeta_E)^{-2} = \int_0^\infty k_E(R) n(R,t)\, dR,$$

$$S_E = \int_0^\infty k_E(R) [\Phi_R(R) - \Psi_E(R)] n(R,t)\, dR. \tag{13}$$

Here, $n(R,t)$ is the density of cylinders per unit length. Owing to the transverse Gaussian shape of the optical quench, one has $\Phi_{\rm el}(r\to\infty) = \Phi_{\rm th}(r\to\infty) = 0$. Thus $\Phi(r\to\infty) = \Phi_0$, i.e., the initial bulk value. Using these boundary conditions, Eq. (11) becomes

$$S_E = D^- (\zeta_E)^{-2} \Phi_0. \tag{14}$$

Moreover, $\Phi_E(r)$ represents the field variation of concentration at steady state. Consequently, using Eq. (12) in the adiabatic approximation [54], i.e., $[\partial\Phi(r)/\partial t] = 0$, the concentration around the cylindrical beam-trapped droplet satisfies

$$[\vec{\nabla}^2-(\zeta_E)^{-2}][\Phi(r)-\Phi_0-\Phi_E(r)]=0. \tag{15}$$

From this equation it appears that ζ_E represents a screening length which removes the divergence at infinity existing in the single cylinder case. Taking into account the boundary conditions, the solution of Eq. (15) is

$$\Phi(r>R)=\Phi_0+\Phi_E(r)+\frac{K_0(r/\zeta_E)}{K_0(R/\xi_E)}\times[\Phi_R(R)-\Phi_0-\Phi_E(R)], \tag{16}$$

where $K_0(x)$ is the zeroth modified Bessel function. Then, we can deduce the cylindrical flux of solute $\vec{J}_C(R)$ at the droplet interface

$$\vec{J}_C(R)=2\pi RlD^-\left\{\left(\frac{\partial\Phi_E}{\partial r}\right)_{r=R}-\frac{1}{\zeta_E}\frac{K_1(R/\zeta_E)}{K_0(R/\zeta_E)}\times[\Phi_R(R)-\Phi_0-\Phi_E(R)]\right\}\frac{\vec{r}}{r}, \tag{17}$$

where $K_1(x)$ is the first modified Bessel function. Using the definitions given by Eq. (10), we also get

$$k_E(R)=2\pi D^-\left(\frac{R}{\zeta_E}\right)\frac{K_1(R/\zeta_E)}{K_0(R/\zeta_E)},$$

$$\Psi_E(R)=\Phi_E(R)+\zeta_E\frac{K_0(R/\zeta_E)}{K_1(R/\zeta_E)}\left(\frac{\partial\Phi_E}{\partial r}\right)_{r=R}. \tag{18}$$

If we assume that the incident beam power is sufficiently low, as in the experiments, to ensure a sufficient optical trapping of the droplet without inducing a field variation of the surface tension σ [55], then $\Phi_R(R)$ is given by the classical Gibbs-Thomson relation for cylinders [52],

$$\Phi_M-\Phi_R(R)=\frac{1}{(\Phi_M-\Phi_m)(\partial\mu/\partial\Phi)_T}\frac{\sigma}{R}, \tag{19}$$

where μ is the chemical potential per unit volume. By mass balance, the flux of solute at the droplet interface equals its volume change,

$$\vec{J}_C(R)=(\Phi_m-\Phi_M)\frac{d}{dt}(\pi R^2l)\frac{\vec{r}}{r}. \tag{20}$$

Then, the transverse three-dimensional diffusion-controlled growth rate of a cylindrical beam-trapped droplet nucleated by an optical quench in composition becomes

$$\frac{dR}{dt}=\frac{D^-}{R}\left(\frac{R}{\zeta_E}\right)\frac{K_1(R/\zeta_E)}{K_0(R/\zeta_E)}\times\left\{\frac{\Phi_E(R)+R\left(\frac{\zeta_E}{R}\right)\frac{K_0(R/\zeta_E)}{K_1(R/\zeta_E)}\left(\frac{\partial\Phi_E}{\partial r}\right)_{r=R}}{\Phi_m-\Phi_M}+\frac{\Phi_0-\Phi_M}{\Phi_m-\Phi_M}-\frac{d_0}{R}\right\}, \tag{21}$$

where ζ_E satisfies the relationship $(\zeta_E)^{-1}=2\pi\int_0^\infty R[K_1(R/\zeta_E)/K_0(R/\zeta_E)]n(R,t)dR$. Here d_0 is a capillary length given by

$$d_0=\frac{\sigma}{(\Phi_m-\Phi_M)^2(\partial\mu/\partial\Phi)_T}. \tag{22}$$

In a ''Φ^4'' model of phase transitions, one has $d_0=\xi^-/6$ [56]. Finally, when comparing the experimental results with the model, we assume that the variation of R/ζ_E with the quench depth calculated numerically by Marqusee for the Ostwald ripening regime still holds in the presence of the laser field.

Equation (21) is very similar to the classical growth rate of a cylindrical domain for spatially uniform quenching [52], except that now, the supersaturation $\Phi_E(R)+R(\zeta_E/R)K_0(R/\zeta_E)/K_1(R/\zeta_E)(\partial\Phi_E/\partial r)_{r=R}+\Phi_0-\Phi_M$ becomes a function of the beam and the droplet radii. Moreover, we now need to particularize $\Phi_E(r)$. In fact, for a better illustration, we will separate the thermodiffusive and the electrostrictive processes, assuming that $\Phi_E(r)$ is either $\Phi_{\rm th}(r)$ or $\Phi_{\rm el}(r)$. Since the phase transition in our experimental system is essentially driven by a thermodiffusive contribution, we will mainly discuss this case and give results for electrostriction when needed. Following the procedure for thermodiffusion, the treatment of an electrostriction-driven transition is totally straightforward. According to Eqs. (2a) and (4), we can write $\Phi_{\rm th}(r)$ as

$$\Phi_{\rm th}(r)=(\Phi_{\rm th})_0\frac{1}{\ln(\gamma(a_{\rm cl}/a_0)^2)}\left\{-E_1\left(\frac{r^2}{a_0^2}\right)-\ln\left(\frac{r^2}{a_{\rm cl}^2}\right)\right\}, \tag{23}$$

where

$$(\Phi_{\rm th})_0=\Phi_{\rm th}(r=0)=-\frac{\varrho_0}{\varrho_S}\frac{k_T}{T_0}\frac{\alpha_a P}{4\pi\Lambda_{\rm th}}\ln\left(\gamma\frac{a_{\rm cl}^2}{a_0^2}\right)$$

is the optical quench in composition on the beam axis and $\gamma=1.781$ is the Euler constant [$E_1(x\ll1)\approx-\ln(\gamma x)+x$].

Without any alteration of generality, we assume $\Phi_0=\Phi_M$ for the description of the model. This means that the initial composition of the mixture is supposed to be located on its coexistence curve as for experiments at $T_0>T_C$. In that case, all the incident beam power is used for the quench. So, by particularizing the optical quench to the thermodiffusive contribution and taking into account $\Phi_0=\Phi_M$, the droplet growth rate becomes

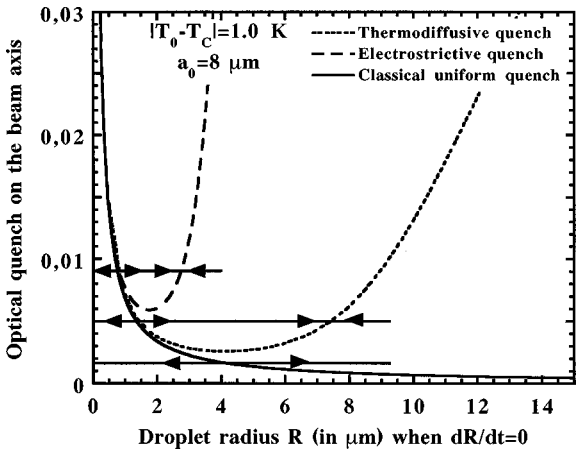

FIG. 11. Set of radii corresponding to a zero growth rate versus the optical quench depth at the beam center for both electrostrictive and thermodiffusive processes. The left (right) part gives the variation of the critical radius R_C^E (maximum radius $R_{\max}^E$) allowed by the finite size of the wave. For a comparison, the variation for a classical uniform quench inside an infinite medium is also plotted. The arrows indicate the evolution of the droplet radius in the different regions separated by $dR/dt=0$.

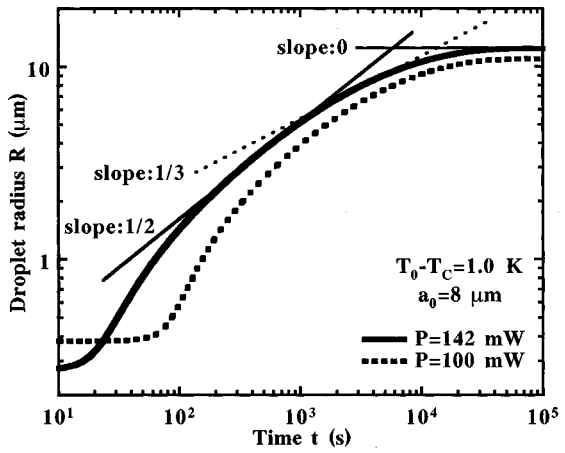

FIG. 12. Predicted droplet growth for the experimental conditions given in Fig. 10 ($P=142$ mW) and for a smaller quench depth ($P=100$ mW). The regimes $R\propto t^{1/2}$ (intermediate free-growth stage) and $R\propto t^0$ (finite-size effects) are depicted. The behavior $R\propto t^{1/3}$ is given for ease of interpretation since it corresponds in the model to a crossover between the predicted $R\propto t^{1/2}$ and $R\propto t^0$ regimes.

$$\frac{dR}{dt}=\frac{D^-}{R}\left(\frac{R}{\zeta_E}\right)\frac{K_1(R/\zeta_E)}{K_0(R/\zeta_E)}\left(\frac{(\Phi_{\rm th})_0}{(\Phi_M-\Phi_m)}\,\frac{1}{\ln(\gamma a_{\rm cl}^2/a_0^2)}\right.$$
$$\left\{-E_1\left(\frac{R^2}{a_0^2}\right)-\ln\left(\frac{R^2}{a_{\rm cl}^2}\right)+2\left(\frac{\zeta_E}{R}\right)\frac{K_0(R/\zeta_E)}{K_1(R/\zeta_E)}\right.$$
$$\left.\left.\times\left[\exp\left(-\frac{R^2}{a_0^2}\right)-1\right]\right\}-\frac{d_0}{R}\right). \tag{24}$$

If $R\ll a_0$, Eq. (24) reduces to the familiar expression of the growth rate in two dimensions for spatially uniform quenches [52]. To show the difference with a classical spatially uniform situation, Fig. 11 illustrates the set of predicted radii for which $dR/dt=0$ versus the quench depth on the beam axis. For a comparison, the electrostrictive case is also depicted [assuming $(\phi_{\rm el})_0=(\Phi_{\rm th})_0$] as well as the classical behavior which, as stated above, corresponds to the situation $R\ll a_0$. In the latter case, $dR/dt=0$ gives the set of critical radii. This set is represented by a hyperbola which simply means that the critical radius is inversely proportional to the quench depth. For an optical quench, the situation is more complicated. In the presence of the wave, the stationary regime $dR/dt=0$ leads to a droplet radius which exhibits a cuvette shape as a function of the initial central quench depth. $dR/dt=0$ is positive inside this curve and negative outside. The left branch corresponds to the critical radius R_C^E variation and the right branch gives the maximum droplet radius $R_{\max}^E$ allowed by the finite size of the optical quench. This finite-size effect also leads to a cutoff in the set of possible R_C^E: There is a maximum value of R_C^E which also represents the smallest accessible $R_{\max}^E$; this is associated with a minimum quench depth below which the transition cannot occur. This limitation shows that the beam size reduces the set of accessible length scales for droplet growth compared to a classical uniform quench.

Moreover, Fig. 11 also illustrates different behaviors, in terms of accessible droplet radii, for an electrostrictive or a thermodiffusive quench in composition. This difference is due to the local or the nonlocal character of the quench. Since electrostriction varies linearly with field intensity, it is highly dependent on the beam radius and droplet radii cannot be larger than a_0. On the contrary, for thermodiffusion, which is driven by the temperature dissipated in the medium and thus essentially depends on the beam power, such a strong dependence does not exist and values of $R_{\max}^E$ larger than the beam radius are allowed. It also explains why in the preceding section the bulk regime $R\propto t^{1/3}$ was observed even for droplet radii larger than the beam radius.

To illustrate the saturation of the droplet radius towards $R_{\max}^E$, and thus the appearance of an $R\propto t^0$ regime at the late stage of the transition, we can compute the droplet growth from Eq. (24). The full line in Fig. 12 illustrates the predicted variation for the experimental conditions given in Fig. 10. Integration was done considering the initial condition $R[\tau_C^E=(R_C^E)^3/D^-\xi^-]=R_C^E+\xi^-/2$, where τ_C^E is the relaxation time associated with the critical radius R_C^E (deduced from $dR/dt=0$) at the beginning of the quench and $\xi^-/2$ corresponds to an uncertainty on the activation barrier of the order of k_BT [56]. The experimental droplet growth saturation is theoretically observed. Moreover, when $R/a_0\ll 1$, the droplet does not feel the Gaussian nature of the quench, and the classical free-growth behavior $R\propto t^{1/2}$ predicted at the intermediate stage in classical situations [57] is also recovered by the model. However, since we are essentially interested in the influence of the finite-size effects on droplet growth, we have not supplemented the droplet growth rate equation by the mass conservation equation [52] (lever rule at thermodynamic equilibrium); this could be done using the procedure developed in Ref. [58] coupled with our predicted growth rate. Thus, even if a sort of $R\propto t^{1/3}$ behavior appears

in the predicted droplet growth, it is not associated with the Ostwald ripening regime (as in experiments) because mass conservation was not taken into account; it corresponds instead to a crossover between the predicted $R \propto t^{1/2}$ and t^0 regimes.

Finally, for the same beam conditions and $|T_0 - T_C|$, we saw in the preceding experimental section that the growth exponent in the bulk regime measured for $T_0 < T_C$ is larger than that for $T_0 > T_C$. Since Φ_0 is not located on the coexistence curve for $T_0 < T_C$, the term $(\Phi_0 - \Phi_M)/(\Phi_m - \Phi_M)$ appearing in the growth rate needs to be considered within the description of our experiments. This means that for the same range of measured droplet radii, the growth rate is smaller when the quench is deeper. To mimic this behavior, we continue to assume $\Phi_0 = \Phi_M$ and decrease the beam power. Figure 12 shows that observations are recovered: in the bulk regime the slope of the droplet growth law decreases when the quench depth increases, because finite-size effects appear earlier.

C. Kinetics of crossover induced by finite-size effects

The kinetics of crossover induced by the finite size of the optical quench was investigated for different experimental conditions. After a first illustration given in Fig. 10 for a beam waist $a_0 = 8\ \mu$m, Figs. 13(a)–13(c) depict in more detail the saturation of the growth of a single beam-trapped droplet for $a_0 = 3\ \mu$m. To analyze the effect of the quench depth, the beam power and the distance in temperature to the critical point were modified. Each figure also gives the predicted $R(t)$ variations. The direct comparison between experiments and predictions is made difficult due to the droplet coalescences occurring at the early stage of the transition. The parts of the data representing the bulk regime of the growth still continue to be larger than those predicted by the model, which is intrinsically diffusion-driven. The transient nature of this droplet growth acceleration, used in the preceding section to recover the number of coalescences observed visually at the beginning of the transition, can easily be checked by making a time translation of the experimental data. The result of this procedure is illustrated in the different insets. As also shown in Table II, the agreement between predicted and measured $R^E_{\max}$ values is quite satisfactory, except for $T_0 - T_C = 0.4$ K (see discussion below). Therefore, these experiments demonstrate that after the coalescence stage, the diffusional nature of the droplet growth in an $l = 100\ \mu$m glass capillary is really preserved in the beam during the late stage of the transition.

We also analyzed finite-size effects in the presence of advection in a cell of optical path $l = 2$ mm (configuration illustrated in Fig. 3). The growth of two flowing droplets in such a geometry is presented in Fig. 14. Even if the existence of the flow makes the data noisy, the droplet radius saturation is observed again and the $R^E_{\max}$ values are in reasonable agreement with those predicted for a pure diffusive growth. Of course, before saturation, the growth ($R \propto t^{0.8}$) cannot fit the predictions because the advection makes the kinetics much faster than a diffusion-driven one [59]. Thus, despite the axial flow of the droplets, the finite transverse size of the beam still constrains the growth, and the $R^E_{\max}$ value seems to correspond to that obtained for a diffusion-controlled kinet-

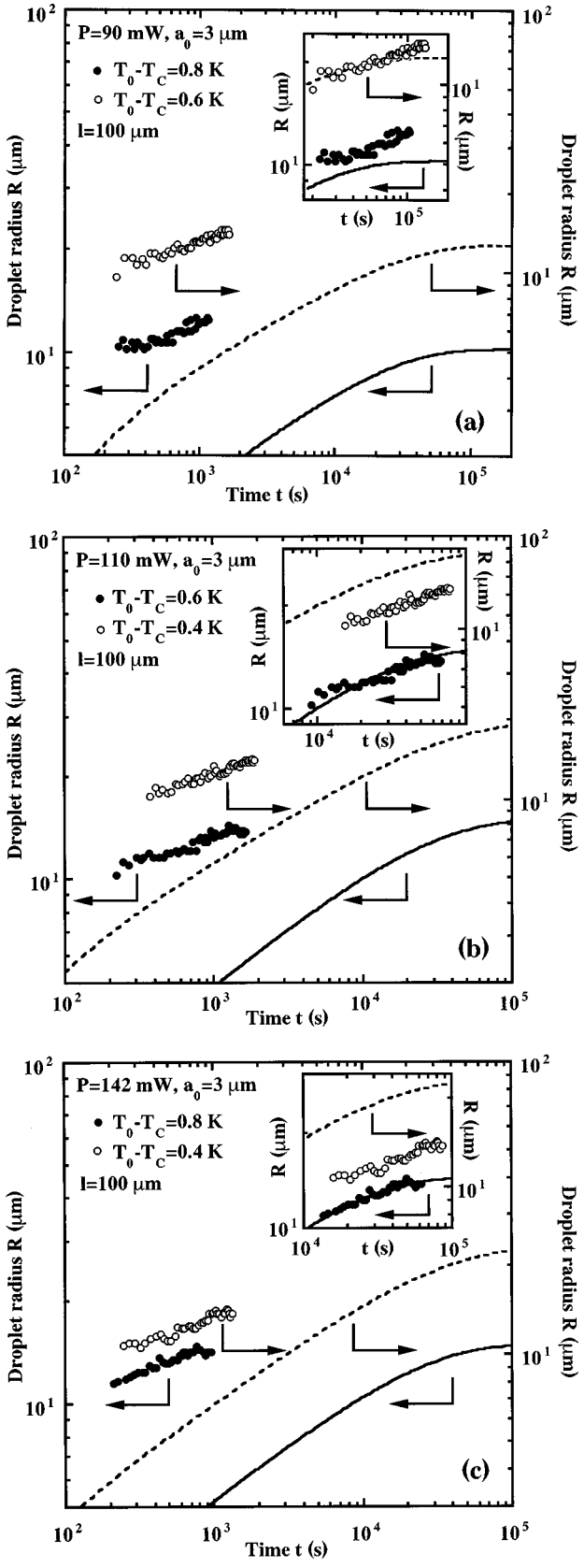

FIG. 13. Finite-size effects on the growth law of a beam-trapped droplet in the 100-μm-thick capillary. Predicted $R(t)$ variations (solid and dashed lines) are also depicted for comparison with experiments. Inset: comparison after a time translation of the experimental points (see text). (a) For $P = 90$ mW, (b) for $P = 110$ mW, and (c) for $P = 142$ mW.

TABLE II. Experimental and predicted values (between parentheses) of the maximum droplet radius $R^E_{\max}$ (in micrometers) resulting from an optical quench in composition as a function of the different external parameters.

	$P=90$ mW $a_0=3$ μm $l=100$ μm	$P=110$ mW $a_0=3$ μm $l=100$ μm	$P=142$ mW $a_0=3$ μm $l=100$ μm	$P=110$ mW $a_0=8$ μm $l=300$ μm	$P=142$ mW $a_0=8$ μm $l=100$ μm* $l=300$ μm† $l=2$ mm$^\#$
$T_0-T_C=0.4$ K	12 ± 1 (16.9)	14 ± 1 (19.5)	14 ± 1 (23)		$16\pm1^\dagger$ (19.2)
$T_0-T_C=0.5$ K				15 ± 1 (14.7)	$17\pm1^\dagger$ (16.9)
$T_0-T_C=0.6$ K	14 ± 1 (12.7)	14 ± 1 (14.9)	15 ± 1 (17.9)		$15\pm1^\dagger$ (15.4)
$T_0-T_C=0.8$ K	12 ± 1 (10.3)	14 ± 1 (12.2)	14 ± 1 (14.8)		$14\pm1^\#$ (13.5)
$T_0-T_C=1.0$ K					14 ± 1* (12.4)

ics. Analyzing all the measured and predicted $R^E_{\max}$ listed in Table II, two conclusions can be made. First, the agreement is reasonably good, except for $T_0-T_C=0.4$ K, for which the measured $R^E_{\max}$ is smaller than the predicted value. Since this discrepancy only appears when T_C is approached, it could be explained by the saturation of thermodiffusion, which also exists for electrostriction, and results from the vicinity of the critical point (see Appendix A in Ref. [31]). Unfortunately, we have never been able to give a definite answer to this hypothesis. Indeed, elimination of the saturation of the field coupling at $T_0-T_C=0.4$ K, if it exists, implies the use of smaller beam intensities, i.e., a decrease in the beam power ($P<90$ mW) or an increase in the beam waist a_0 ($a_0>8$ μm). However, in both cases, the beam intensity was not sufficiently strong to allow an efficient beam trapping. On the other hand, despite the continuous advection of the growing droplets in cells of optical path $l=2$ mm (droplet velocity $V_d\approx1$ μm/s), the measured $R^E_{\max}$ values surprisingly correspond to those obtained from the model, even if the growth rate is much larger: in the bulk regime one has $R\propto t^{0.8}$ instead of $R\propto t^{1/3}$. This simply means that at low Reynolds number, here $\mathrm{Re}\approx2\times10^{-6}$ for a droplet radius $R=10$ μm, the flow is too weak to disturb the intrinsic cutoff distance imposed by the beam.

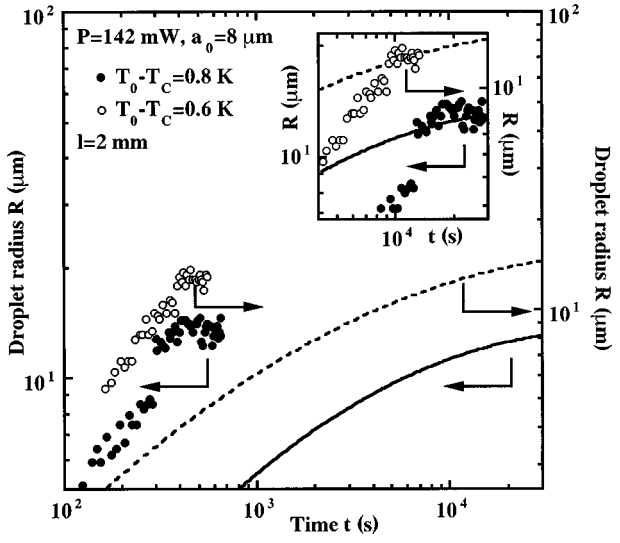

FIG. 14. Finite-size effects on the growth law of a droplet flowing along the beam axis in the cell (2 mm thick). Predicted $R(t)$ variations (solid and dashed lines) are also depicted for comparison with experiments. Inset: comparison after a time translation of the experimental points (see text).

Finally, thermodynamic stability means that a droplet of radius larger than $R^E_{\max}$ is unstable. It should evaporate until its radius reaches $R^E_{\max}$. This expected behavior can be experimentally checked in a capillary of optical path $l=300$ μm. Indeed, unlike the situation depicted in Fig. 5 for $l=100$ μm, when $l=300$ μm two droplets generally remain in the capillary at the late stage of the transition. Since they eventually coalesce, the radius of the resulting final droplet becomes larger than $R^E_{\max}$. Figure 15 illustrates the expected droplet evaporation and the decrease in its radius towards $R^E_{\max}$ for different values of the control parameters. The coalescences, indicated by an arrow, are clearly evidenced by the shifts in droplet radius. Also represented are the predicted diffusion-driven $R(t)$ variations. For this capillary size, a weak droplet advection also appears, now transiently, at the intermediate stage of growth. As previously shown for $l=2$ mm, we can again observe that (i) $R^E_{\max}$ seems to be insensitive to the transient flow and (ii) before saturation, the growth law is $R\propto t^{0.8}$.

D. Discussion of finite-size effects

The above analysis shows that the cutoff distance imposed by the beam radius breaks the universal behavior of droplet growth [2] as soon as the drop starts to feel the beam size. A direct comparison with recent theoretical work on finite-size effects in phase-separating systems [47,48] is, however, difficult to make, particularly because of the ''soft wall'' geometry provided by the wave. The shape of the beam generates a cutoff volume, with no rigid boundary, beyond which the transition cannot occur. Unlike classical situations, the size of this volume varies with the amplitude of the different control parameters ($P,a_0,|T-T_C|$). Moreover, the initial quench is not spatially uniform over this length scale. Thus, finite-size effects induced by a laser wave are quite different from those resulting from the rigid boundary conditions used in Refs. [47,48]. First, in a Gaussian quench there is no need for additional hypotheses taking into account the finiteness of the box containing the medium, either by imposing a cutoff droplet radius on the growth rate

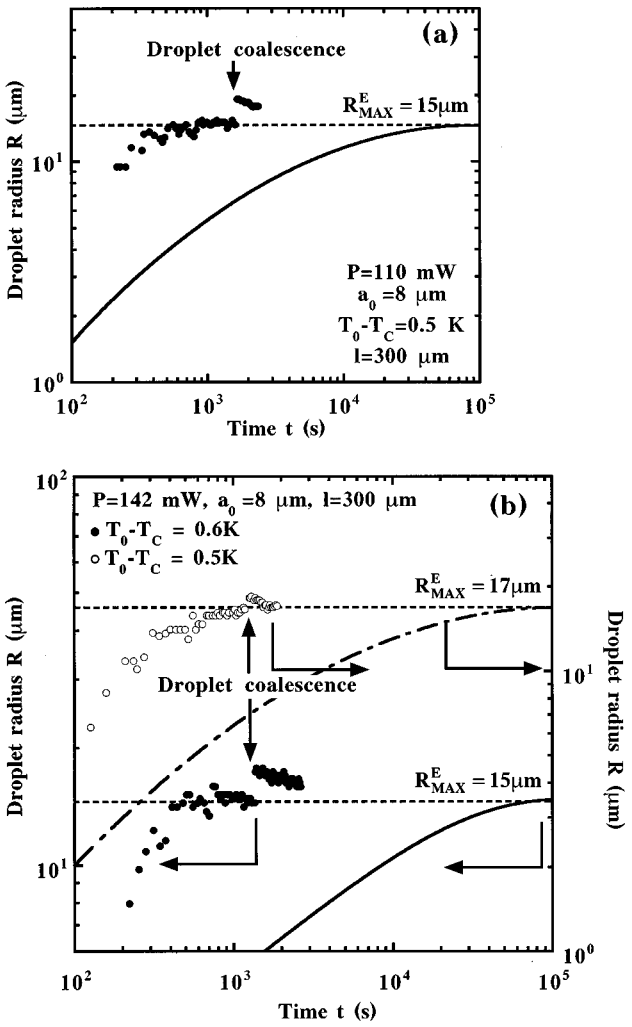

FIG. 15. Illustration of the thermodynamic stability of the $R^E_{\max}$ value by the decrease in the droplet radius R ($>R^E_{\max}$) towards $R^E_{\max}$ after the coalescence with a second droplet (indicated by the arrow). The predicted droplet growths (solid line) are also illustrated. (a) For $P=110$ mW and (b) for $P=142$ mW.

[48] or by using a lever rule for a finite volume [47]. Indeed, even if the wave creates a length scale beyond which the transition cannot be induced, both the medium and the Gaussian excitation are still of infinite extent. On the other hand, a description of the droplet distribution, as in Refs. [47,48], does not really hold for an optical quench since only a few droplets are nucleated in the beam.

Therefore, this study illustrates how finite-size effects can be smoothly induced in a bulk material to prevent abrupt boundary conditions. It also describes a new way to analyze these effects experimentally in a wetting-free geometry, since it is well known that the preferential attraction of one of the two coexisting phases on the rigid boundaries results in a dynamic coupling between the growth and wetting phenomena, which considerably modifies the kinetics of coarsening [60].

V. CONCLUSION

In this paper we have investigated the late stage kinetics of first-order phase transitions in liquid mixtures driven by a cw laser wave. Our main aim was to illustrate how finite-size effects can be explored in fluids, whereas classical methods fail due to the impossibility of eliminating the intrinsic interaction with the container. Since the wave behaves in a bulk as an optical bottle with ''soft walls,'' we show that laser-induced transitions fulfill their promise. Moreover, to incorporate such an analysis in a more general framework, it is also important to compare the field-induced kinetics in the absence of finite-size effects with classical results obtained in familiar uniform quench situations.

In a near-critical micellar phase of microemulsion we have illustrated the ability of laser waves to quench a mixture in composition, to nucleate droplets of the minority phase, and to trap them optically. Working with small optical path cells, the growth of a single droplet in compensated gravity has been investigated. In a first step, we analyzed the bulk behavior of this droplet growth. The classical behavior $R \propto t^{1/3}$ was recovered. To interpret the amplitude of the measured growth laws, the data were analyzed in terms of reduced length and time scales for the Ising class ($d=3,n=1$). This description shows that the droplet growth driven by the wave when finite-size effects are negligible is in total agreement with the behavior observed in classical situations.

To pursue this investigation, we extended this study to the intrinsic influence of the finite size of the beam on the droplet growth. After a first illustration of the crossover from the $R \propto t^{1/3}$ regime to the saturation of the kinetics associated with the decrease in quench depth felt by the growing droplet, we developed a model of growth inside the beam. The dynamics in the presence of the wave was calculated and the kinetics of crossover induced by finite-size effects is described. Our experiments are interpreted using this model. Despite some approximations, there is good quantitative agreement between theory and experiments. We also illustrate the robustness of finite-size effects, showing that they are not disturbed by the advection of the growing droplets at low Reynolds numbers even if the growth laws are modified by the flow.

As a consequence, the present work shows how laser waves can be used to investigate the kinetics of conserved-order-parameter first-order phase transitions whereas more classical experimental setups are limited. More generally, this new application of laser waves illustrates their efficiency to induce localized gradients in the bulk and to control non-equilibrium processes in soft matter physics.

ACKNOWLEDGMENTS

We are grateful to E. Freysz and Y. Garrabos for helpful discussions, and J. Plantard and M. Winckert for technical assistance. This work was partially supported by the Région Aquitaine.

[1] J. D. Gunton, M. San Miguel, and P. S. Sahni, in *Phase Transition and Critical Phenomena*, edited by C. Domb and J. L. Lebowitz (Academic, New York, 1983), Vol. 8.
[2] A. J. Bray, Adv. Phys. **43**, 357 (1994).
[3] V. Schmitt, C. M. Marques, and F. Lequeux, Phys. Rev. E **52**, 4009 (1995).
[4] K. Fujioka, T. Takebe, and T. Hashimoto, J. Chem. Phys. **98**, 717 (1993), and references cited therein.
[5] B. J. Ackerson and N. A. Clark, Phys. Rev. A **30**, 906 (1984).
[6] T. Hashimoto, K. Matsuzaka, E. Moses, and A. Onuki, Phys. Rev. Lett. **74**, 126 (1995).
[7] K. Y. Min and W. I. Goldburg, Phys. Rev. Lett. **70**, 469 (1993); **71**, 569 (1993).
[8] E. Helfand and G. H. Fredrickson, Phys. Rev. Lett. **62**, 2468 (1989); S. T. Milner, *ibid.* **66**, 1477 (1991).
[9] Bubbles 40, Proceedings of the Conference on the Bubble Chamber and Its Contributions to Particle Physics, edited by G. G. Harigel, D. C. Colley, and D. C. Cundy [Nucl. Phys. B **36**, (1993)].
[10] P. Debye and K. Kleboth, J. Chem. Phys. **42**, 3155 (1965).
[11] P. Debye, C. C. Gravatt, and M. Ieda, J. Chem. Phys. **46**, 2352 (1967).
[12] D. Wirtz and G. G. Fuller, Phys. Rev. Lett. **71**, 2236 (1993).
[13] A. Onuki, Physica A **217**, 38 (1995), and references cited therein; **221**, 565(E) (1995).
[14] D. S. Parmar and B. Labroo, Phys. Lett. **88A**, 466 (1982).
[15] K. J. Cheng, Phys. Lett. **106A**, 403 (1984).
[16] P. L. Marston and R. E. Apfel, Phys. Lett. **60A**, 225 (1977).
[17] K. J. Cheng and J. B. Chaddock, Int. J. Heat Fluid Flow **7**, 278 (1986).
[18] C. G. Garton and Z. Krasuchi, Proc. R. Soc. London, Ser. A **280**, 211 (1964).
[19] K. J. Cheng and J. B. Chaddock, Int. Comm. Heat Mass Transfer **12**, 259 (1985).
[20] K. Y. C. Lee, J. F. Klinger, and H. M. McConnell, Science **263**, 655 (1994).
[21] B. Ward and D. C. Emmony, Appl. Phys. Lett. **59**, 2228 (1991).
[22] S. F. Rastopov and A. T. Sukhodol'ski, Phys. Lett. A **149**, 229 (1990).
[23] B. A. Garetz, J. E. Aber, N. L. Goddard, R. G. Young, and A. S. Myerson, Phys. Rev. Lett. **77**, 3475 (1996).
[24] A. I. Sheifot and M. N. Gaidukov, Sov. Phys. Tech. Phys. **31**, 581 (1986).
[25] J. Hofkens, J. Hotta, K. Sazaki, H. Masujara, and K. Iwai, Langmuir **13**, 414 (1997).
[26] P. Borowicz, J. Hotta, K. Sazaki, and H. Masujara, J. Phys. Chem. B **101**, 5900 (1997).
[27] J. P. Delville, C. Lalaude, E. Freysz, and A. Ducasse, Phys. Rev. E **49**, 4145 (1994).
[28] A. J. Palmer, Opt. Lett. **5**, 54 (1980).
[29] M. Giglio and A. Vendramini, Phys. Rev. Lett. **34**, 561 (1975); **38**, 26 (1977).
[30] C. Lalaude, J. P. Delville, S. Buil, and A. Ducasse, Phys. Rev. Lett. **78**, 2156 (1997).
[31] B. Jean-Jean, E. Freysz, A. Ponton, A. Ducasse, and B. Pouligny, Phys. Rev. A **39**, 5268 (1989); B. Jean-Jean, E. Freysz, A. Ducasse, and B. Pouligny, Europhys. Lett. **7**, 219 (1988).
[32] D. Gazeau, E. Freysz, and A. M. Bellocq, Europhys. Lett. **9**, 833 (1989).
[33] A. Ashkin, J. M. Dziedzic, J. E. Bjorkholm, and S. Chu, Opt. Lett. **11**, 288 (1986).
[34] J. P. Delville, C. Lalaude, Y. Garrabos, and A. Ducasse (unpublished).
[35] F. Perrot, P. Guenoun, T. Baumberger, D. Beysens, Y. Garrabos, and B. Le Neindre, Phys. Rev. Lett. **73**, 688 (1994).
[36] M. Seul, N. Y. Morgan, and C. Sire, Phys. Rev. Lett. **73**, 2284 (1994).
[37] O. Krishevsky and J. Stavans, Phys. Rev. Lett. **70**, 1473 (1993); Phys. Rev. E **52**, 1818 (1995).
[38] H. M. Lai, P. T. Leung, K. L. Poon, and K. Young, J. Opt. Soc. Am. B **6**, 2430 (1989).
[39] C. Lalaude, J. P. Delville, Y. Garrabos, E. Freysz, and A. Ducasse, J. Phys. IV **5**, C3-267 (1995).
[40] P. Guenoun, R. Gastaud, F. Perrot, and D. Beysens, Phys. Rev. A **36**, 4876 (1987).
[41] Y. C. Chou and W. I. Goldburg, Phys. Rev. A **20**, 2105 (1979).
[42] H. L. Snyder and P. Meakin, J. Chem. Phys. **79**, 5588 (1983).
[43] H. Furukawa, Adv. Phys. **34**, 703 (1985).
[44] K. Kawasaki and T. Ohta, Prog. Theor. Phys. **59**, 362 (1978).
[45] E. D. Siggia, Phys. Rev. A **20**, 595 (1979).
[46] Y. Garrabos, B. Le Neindre, P. Guenoun, B. Khalil, and D. Beysens, Europhys. Lett. **19**, 491 (1992).
[47] D. W. Heermann, L. Yixue, and K. Binder, Physica A **230**, 132 (1996).
[48] V. V. Slezov, J. Schmelzer, and J. Möller, J. Cryst. Growth **132**, 419 (1993).
[49] J. P. Delville, E. Freysz, and A. Ducasse, Phys. Rev. E **53**, 2488 (1996).
[50] S. Puri, K. Binder, and S. Dattagupta, Phys. Rev. B **46**, 98 (1992).
[51] K. Tsumuraya and Y. Miyata, Acta Metall. **31**, 437 (1983).
[52] J. A. Marqusee, J. Chem. Phys. **81**, 976 (1984).
[53] J. P. Delville, C. Lalaude, and A. Ducasse, Physica A **262**, 40 (1999).
[54] S. R. Corriel and R. L. Parker, J. Appl. Phys. **36**, 632 (1965).
[55] L. Liggieri, A. Sanfeld, and A. Steinchen, Physica A **206**, 299 (1994).
[56] J. S. Langer and A. J. Schwartz, Phys. Rev. A **21**, 948 (1980).
[57] A. Cumming, P. Wiltzius, and F. S. Bates, Phys. Rev. Lett. **65**, 863 (1990); A. Cumming, P. Wiltzius, F. S. Bates, and J. H. Rosedale, Phys. Rev. A **45**, 885 (1992).
[58] A. Nakahara, T. Kawakatsu, and K. Kawasaki, J. Chem. Phys. **99**, 9853 (1993).
[59] T. Baumberger, F. Perrot, and D. Beysens, Phys. Rev. A **46**, 7636 (1992).
[60] H. Tanaka, Phys. Rev. Lett. **70**, 2770 (1993).